Available online at www.sciencedirect.com
SCIENCE DIRECT®
Journal of Computational Physics 200 (2004) 412–431
JOURNAL OF COMPUTATIONAL PHYSICS
www.elsevier.com/locate/jcp

Implicit subgrid-scale modeling by adaptive deconvolution

N.A. Adams *, S. Hickel, S. Franz

Institut für Strömungsmechanik, Technische Universität Dresden, D-01062 Dresden, Germany

Received 3 February 2004; received in revised form 16 April 2004; accepted 16 April 2004
Available online 21 July 2004

Abstract

A new approach for the construction of implicit subgrid-scale models for large-eddy simulation based on adaptive local deconvolution is proposed. An approximation of the unfiltered solution is obtained from a quasi-linear combination of local interpolation polynomials. The physical flux function is modeled by a suitable numerical flux function. The effective subgrid-scale model can be determined by a modified-differential equation analysis. Discretization parameters which determine the behavior of the implicit model in regions of developed turbulence can be adjusted so that a given explicit subgrid-scale model is recovered to leading order in filter width. Alternatively, improved discretization parameters can be found directly by evolutionary optimization. Computational results for stochastically forced and decaying Burgers turbulence are provided. An assessment of the computational experiments shows that results for a given explicit subgrid-scale model can be matched by computations with an implicit representation. A considerable improvement can be achieved if instead of the parameters matching an explicit model discretization parameters determined by evolutionary optimization are used.

AMS: 65M99; 76F65; 76M25

Keywords: Large-eddy simulation; Deconvolution; Subgrid-scale modeling

1. Introduction

The original intention of subgrid-scale modeling was to stabilize under-resolved flow simulations while preserving reasonable accuracy on the resolved scales. By this motivation [1] the most widely used subgrid-scale (SGS) model, the Smagorinsky model, was introduced [2]. While large-scale computations became gradually easier, computational investigations of SGS models intensified, and limitations of the Smagorinsky model were revealed. Improved versions of the Smagorinsky model were constructed by introducing the concept of a dynamic constant and by combining the Smagorinsky model with other models. A comprehensive account of these activities can be found in the recent book of Sagaut [3].

* Corresponding author. Tel.: +49-351-463-37607; fax: +49-351-463-35246.
E-mail address: Nikolaus.Adams@ism.mw.tu-dresden.de (N.A. Adams).

0021-9991/$ - see front matter
doi:10.1016/j.jcp.2004.04.010

Theoretical SGS-model development is mainly based on the filtering approach [4] to large-eddy simulation (LES) where filtering of the underlying conservation law and the subsequent discretization of the filtered conservation law are separated. We call *explicit SGS models* such models which provide explicit approximations or estimations of the unclosed SGS terms obtained after filtering. Explicit SGS models require the *explicit* computation of SGS-stress approximations during time advancement. In particular for compressible flows the computational overhead can be significant. Recent developments of explicit SGS models include attempts to reconstruct directly a part of the unfiltered field such as the estimation model [5] and the approximate deconvolution model [6]. A review of these approaches is given in [7]. A common feature of these models is that they employ an explicit filter operation whose effective filter cut-off wavenumber ξ_C can be adjusted $0 \leqslant \xi_C \leqslant \xi_h$ [8]. With ξ_h we indicate the largest wavenumber which can be represented on the underlying grid with grid spacing h, the Nyquist wavenumber. An analysis of the interference between numerical discretization and subgrid-scale model revealed a clear dependence of ξ_C on the order of accuracy and the resolution properties of the chosen discretization scheme [9].

First theoretical analyses of the mutual interference of SGS model and truncation error of the numerical discretization lead to the conclusion that for SGS-model terms to dominate over the truncation error for standard finite-difference schemes at least fourth-order accuracy is required [10]. These theoretical results were corroborated by numerical simulations [11]. The alternative to higher-order schemes is to increase the distance between ξ_C and ξ_h [9], which can lead, however, easily to one order-of-magnitude increase of computational cost. For LES of flows in complex geometries the use of higher-order schemes leads to implementational complications and computational overhead which one tries to avoid whenever possible.

The interference of SGS model and truncation error can also be beneficial, however. First indications that the truncation error of a linear upwind scheme in some cases may function as *implicit* SGS model, i.e. a SGS model whose terms are not explicitly modeled or computed, were reported by Kawamura and Kuwahara [12]. More generally, the use of nonlinearly stable schemes for implicit LES, i.e. LES with implicit SGS model, was proposed by Boris et al. [13]. Originating from the use of monotone schemes this approach has been dubbed MILES for Monotonically integrated LES, although in practice schemes satisfying less restrictive stability constraints are used. For the latter reason the term implicit LES (ILES) appears to be more appropriate. Noteworthy are in particular the application of the piecewise parabolic method to turbulence by Porter et al. [14] and the so-called multidimensional positive definite advection transport algorithm (MPDATA) method of Smolarkiewicz and Margolin [15,16]. Most intensely the flux-corrected transport (FCT) method was used in the recent past for which considerable success in predicting wall-bounded turbulence was reported by Fureby and Grinstein [17] (see also references therein). On the other hand, the application of off-the-shelf non-oscillatory schemes to isotropic turbulence is less than straightforward, as reported by Garnier et al. [18]. This uncertainty has stimulated a deeper analysis of non-oscillatory discretizations. The most suitable vehicle for analyzing a numerical scheme with respect to its implicit SGS modeling capabilities appears to the be modified-differential equation analysis (MDEA), e.g. [19]. The FCT scheme was analyzed with this method by Fureby et al. [20], the MPDATA method by Margolin and Rider [21].

Following an earlier suggestion [22] the objective of this paper is to design a nonlinear discretization based on standard approaches in such a way that the truncation error provides a suitable implicit SGS model. Computations with the constructed implicit SGS model should produce results at least as good as common explicit models. The benefit lies mainly in the implicit character of the model which removes the computational and a significant part of the implementational complications of explicit SGS models. As mentioned before, for the construction of explicit SGS models filtering of the underlying conservation law and the subsequent discretization are considered separately. For the construction of implicit SGS models, however, we follow the concept of Schumann [23] and consider discretization and filtering simultaneously.

An appropriate framework for connecting filtering and discretization of the underlying conservation law is available by the finite-volume method [19]. We consider now for simplicity the initial-value problem for a generic scalar nonlinear transport equation for the variable v

$$\frac{\partial v}{\partial t}+\frac{\partial F(v)}{\partial x}=0. \tag{1}$$

On a mesh $x_j = jh$ with equidistant spacing h and $j = \ldots, -1, 0, 1, \ldots$ the grid function $v_N = \{v_j\}$ represents a discrete approximation of $v(x)$ by $v_j \doteq v(x_j)$. A spectrally accurate interpolant of the grid function with the same Fourier transform can be constructed using the Whittaker cardinal function [24]. For finite h the representation of the continuous solution $v(x)$ by the grid function v_N results in a subgrid-scale error

$$\mathscr{G}_\mathrm{SGS}=\frac{\partial F_\mathrm{N}(v_\mathrm{N})}{\partial x}-\frac{\partial F_\mathrm{N}(v)}{\partial x} \tag{2}$$

which arises from the nonlinearity of $F(v)$. The modified-differential equation for v_N is

$$\frac{\partial v_\mathrm{N}}{\partial t}+\frac{\partial F_\mathrm{N}(v_\mathrm{N})}{\partial x}=\mathscr{G}_\mathrm{SGS}. \tag{3}$$

A finite-volume discretization of Eq. (1) corresponds to a convolution with the top-hat filter

$$G(x-x_j;h)=\begin{cases}1/h, & |x-x_j|\leqslant h/2,\\ 0, & \text{else}\end{cases} \tag{4}$$

on the grid $x_\mathrm{N} = \{x_j\}$. An application of the filter operation (4) to a function $u(x)$ returns the filtered solution in terms of a grid function u_j at x_j

$$\bar{u}_j = G * u = \frac{1}{h}\int_{x_{j-1/2}}^{x_{j+1/2}} u(x')\,\mathrm{d}x'.$$

The resulting finite-volume approximation of Eq. (1) is given by

$$\frac{\partial \bar{u}_\mathrm{N}}{\partial t}+G*\frac{\partial \tilde{F}_\mathrm{N}(\tilde{u}_\mathrm{N})}{\partial x}=0, \tag{5}$$

where $\tilde{u}_\mathrm{N} \doteq u_\mathrm{N}$ results from an approximate inversion of the filtering $\bar{u}_\mathrm{N} = G * u$.

Although the inverse-filtering operation is ill-posed, an approximation $\tilde{u}_\mathrm{N}$ of u on the grid x_N can be obtained by regularized deconvolution [7]. For a brief summary on the deconvolution concept for subgrid-scale modeling it is illustrative to consider the Fourier-transform $\hat{G}(\xi)$ of G. The filtering operation (4) damps each wavenumber and truncates at the Nyquist wavenumber ξ_h (constant grid spacing assumed). If an inverse operator would exist it could be written in Fourier space simply as $\hat{G}^{-1}(\xi)$. Since $\hat{G}(\xi) = 0$ for $|\xi| \geqslant \xi_h$ only wavenumber contributions $|\xi| < \xi_h$ to the filtered solution can be inverted. This is the regularized deconvolution obtained by singular-value decomposition. For turbulent flows it turned out that this type of regularization is inferior to the van Cittert approach (see [6]) where a linear approximate deconvolution operator is defined from

$$\tilde{u}_\mathrm{N} = \tilde{G}^{-1} * \bar{u}_\mathrm{N} = \left(\sum_{v=0}^{M}(I-G)^v\right) * \bar{u}_\mathrm{N}.$$

The series expansion for the inverse operator on the right-hand side is truncated at M which regularizes the inverse, where M is a (weakly) problem dependent regularization parameter [6,7]. An explicit SGS model based on this linear approximate deconvolution operation was proposed by Stolz and Adams [6] and applied to several canonical flow configurations, e.g. [25]. For most applications of these linear deconvolution operations to flows at large Reynolds numbers an additional relaxation-type regularization of the underlying conservation law was found to be necessary, e.g. [25,26]. In this paper we propose a regulari-

zation based on adusting nonlinearly the local interpolation polynomials to the solution properties. By this extension of the deconvolution operation $\tilde{u}_N = \tilde{G}^{-1} * \bar{u}_N$ to a solution-adaptive nonlinear formulation it is expected that an additional regularization such as in [25,26] can be avoided. Another utensil which can be exploited is the choice of an appropriate and consistent numerical flux function $\tilde{F}_N$ which approximates F_N. In summary, the construction of an implicit SGS model which we propose here amounts to develop an adaptive approximate deconvolution operator $\tilde{G}^{-1}$ and to devise a suitable numerical flux function $\tilde{F}_N$.

Once deconvolution operation and numerical flux function are determined, the MDEA of Eq. (5) leads to an evolution equation of $\bar{u}_N$ in the form of

$$\frac{\partial \bar{u}_N}{\partial t} + G * \frac{\partial F_N(u_N)}{\partial x} = \mathscr{G}_N, \tag{6}$$

where

$$\mathscr{G}_N = G * \frac{\partial F_N(u_N)}{\partial x} - G * \frac{\partial \tilde{F}_N(\tilde{u}_N)}{\partial x} \tag{7}$$

is the truncation error of the discretization. If $\mathscr{G}_N$ approximates $\bar{\mathscr{G}}_{SGS}$ in some sense for *finite h* we obtain an implicit SGS model contained within the discretization. Note that this requirement is different from the requirement of $\mathscr{G}_N$ approximating $\bar{\mathscr{G}}_{SGS}$ for $h \to 0$, which would dictate a spectrally convergent discretization as optimum.

2. Approximate deconvolution

Consistently with the finite-volume approach we will call x_j the cell centers and $x_{j\pm1/2}$ the cell faces of cell j. Filtering (4) applied to the flux derivative $\partial F(u)/\partial x$ in Eq. (1) returns

$$G * \frac{\partial F(u)}{\partial x} = \frac{F(u_{j+1/2}) - F(u_{j-1/2})}{h},$$

which requires an approximation of the unfiltered solution $u(x)$ at the left and right faces of each cell j which are called $u^+_{j-1/2}$ and $u^-_{j+1/2}$, respectively.

The use of a top-hat filter G according to Eq. (4) allows for a primitive-function reconstruction of $u(x)$ from $\bar{u}_N$ at $x_{j\pm1/2}$ as proposed by Harten et al. [27]. In this reference also a more general deconvolution reconstruction was proposed which can be formulated for any graded filter for which sufficiently many filter moments exist. Since the latter procedure results in an increased computational overhead and the advantage of using filters other than the top-hat filter is unclear we restrict ourselves to the top-hat filter and resort to the primitive-function reconstruction in the following. In [27] reconstruction was combined with an interpolation-stencil selection, leading to the essentially non-oscillatory (ENO) property of the reconstructed solution. This procedure is a way of getting a *nonlinear* approximate or regularized deconvolution of the filtered solution.

We extend now the essentially non-oscillatory approach of adaptive deconvolution in such a way that by adjusting discretization parameters implicit SGS models for LES are obtained. For this purpose we introduce a set of interpolation polynomials of order $k = 1, \ldots, K$, for each k with shift $r = 0, \ldots, k-1$ of the left-most stencil point which also identifies the respective stencil. Admissible stencils, i.e. stencils which include the interpolation points $x_{j\pm1/2}$ in their support, range from from $j - r$ to $j - r + k - 1$, expressed by (k, r). The stencil setup is illustrated in Fig. 1. Right-face interpolants at $x_{j+1/2}$ and left-face interpolants at $x_{j-1/2}$ of order k are given by Eq. (2.10) of [28]

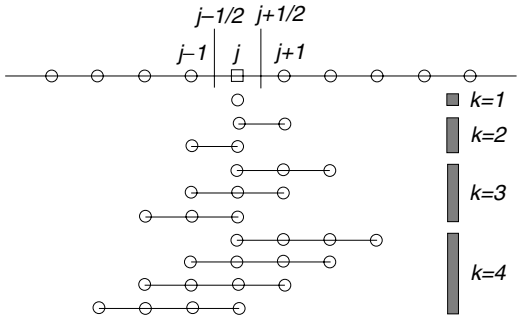

Fig. 1. Admissible stencils for polynomial order $k = 1, 2, 3, 4$.

$$p^{-}_{k,r}(x_{j+1/2}) = \sum_{l=0}^{k-1} c^{(k)}_{r,l}(j)\bar{u}_{j-r+l}, \quad p^{+}_{k,r}(x_{j-1/2}) = \sum_{l=0}^{k-1} c^{(k)}_{r-1,l}(j)\bar{u}_{j-r+l}, \tag{8}$$

respectively. For each k these expressions represent the information contained in admissible polynomials, where deconvolution and interpolation are expressed by the coefficients $c^{(k)}_{r,l}(j)$. A rule for computing these coefficients is given by Eq. (2.20) of [28]

$$c^{(k)}_{r,l}(j) = h_{j-r+l} \sum_{\mu=l+1}^{k} \frac{\sum_{p=0}^{k} \prod_{\substack{v=0 \\ p\neq\mu v\neq\mu,p}}^{k} x_{j+1/2} - x_{j-r+v-1/2}}{\prod_{\substack{v=0 \\ v\neq\mu}}^{k} x_{j-r+\mu-1/2} - x_{j-r+v-1/2}}. \tag{9}$$

As indicated, this rule holds for variable mesh spacing. If $h_j = h = const.$ it can be simplified accordingly [28]. The index range of $c^{(k)}_{r,l}(j)$ is $r = 0, \ldots, k-1$ and $l = 0, \ldots, k-1$ for each $k = 1, \ldots, K$.

For ENO or weighted-ENO (WENO) approaches [29] a single interpolation-polynomial order is chosen. Here, we construct a quasi-linear combination of all possible interpolation polynomials according to Eq. (8) up to a certain order K

$$\tilde{u}^{\mp}_{j\pm1/2} = \sum_{k=1}^{K} \sum_{r=0}^{k-1} \omega^{\mp}_{k,r}(j) p^{\mp}_{k,r}(x_{j\pm1/2}). \tag{10}$$

As restriction we impose that the sum of all weights $\omega^{\pm}_{k,r}(j)$ over k and r is unity

$$\sum_{k=1}^{K} \sum_{r=0}^{k-1} \omega^{\pm}_{k,r} = 1.$$

Eq. (10) gives the resulting approximants for the deconvolved solution at the left and right cell faces.

Finally, an appropriate numerical flux function $\tilde{F}_{\mathrm{N}}$ needs to be devised which approximates the physical flux F. One choice is a modified Lax–Friedrichs flux function

$$\tilde{F}_{\mathrm{N}}(x_{j+1/2}) = \frac{1}{2}\left(F(\tilde{u}^{-}_{j+1/2}) + F(\tilde{u}^{+}_{j+1/2})\right) - \sigma_{j+1/2}\left(\tilde{u}^{+}_{j+1/2} - \tilde{u}^{-}_{j+1/2}\right),$$

where $\sigma_{j+1/2}$ can be any shift-invariant functional of $\bar{u}_{\mathrm{N}}$. During computational experimentation we found that the following numerical flux function for our purposes leads to favorable error cancellations:

$$\tilde{F}_{\mathrm{N}}(x_{j+1/2}) = F\left(\frac{\tilde{u}^{-}_{j+1/2} + \tilde{u}^{+}_{j+1/2}}{2}\right) - \sigma_{j+1/2}\left(\tilde{u}^{+}_{j+1/2} - \tilde{u}^{-}_{j+1/2}\right). \tag{11}$$

The implicit SGS model is expressed in the above framework by the choices for the smoothness measure which enters the computation of $\omega^{\pm}_{k,r}$ and the dissipative weights $\sigma_{j+1/2}$. For the weights $\omega^{\pm}_{k,r}$ we follow the WENO approach [29] and set

$$\omega^{\pm}_{k,r} = \frac{1}{K}\frac{\alpha^{\pm}_{k,r}}{\sum_{\mu=0}^{k-1}\alpha^{\pm}_{k,\mu}}. \tag{12}$$

The coefficients $\alpha^{\pm}_{k,r}$ are computed from

$$\alpha^{\pm}_{k,r} = \gamma^{\pm}_{k,r}(\varepsilon + \beta_{k,r})^{-2}, \tag{13}$$

where ε is a small number to prevent singularity. The smoothness measure $\beta_{k,r}$ is computed as the total variation (TV) of $\tilde{u}_{\mathrm{N}}$ on the considered stencil

$$\beta_{k,r} = \sum_{\mu=-r}^{k-r-2} |\bar{u}_{j+\mu+1} - \bar{u}_{j+\mu}|. \tag{14}$$

Alternatively, the WENO smoothness measure as proposed by Jiang and Shu [30] can be chosen, see e.g. Eqs. (2.61)–(2.63) of [28].

The dissipative weight in Eq. (11) can be chosen, e.g., as $\sigma_{j+1/2} = |\bar{u}_{j+1} - \bar{u}_j|$. Eq. (13) introduces free parameters for the right-face interpolant $\gamma^{-}_{k,r}$ and the left-face interpolant $\gamma^{+}_{k,k-1-r}$, which are constrained to be symmetric with respect to the stencil center $\gamma^{-}_{k,r} = \gamma^{+}_{k,k-1-r}$. Objective of implicit SGS modeling is to determine these parameters which close the model.

3. Implicit subgrid-scale model derivation and analysis

The MDEA is performed here for the semi-discretization only. This is consistent with the spatially filtered interpretation of the LES equations, the time step being sufficiently small for the spatial truncation error to be dominant. Based on the results of Section 3.1.3 we argue that this is indeed the case for a time-step size chosen according to the Courant–Friedrichs–Lewy limit

$$\tau = h\frac{\mathrm{CFL}}{\max_x \partial F/\partial v}. \tag{15}$$

For time integration we have tested two different explicit Runge–Kutta schemes, as detailed below. For implicit time integrations or larger time-step sizes an extension of MDEA to full discretizations should be considered. In this case, however, the LES is in effect space and time filtered [31]. For all computations the diffusive terms are discretized by a fourth-order central finite difference.

The central assumption for performing the MDEA is that the discrete unfiltered solution u_{N} in a neighborhood of x_j can be represented by local approximation polynomials of degree K up to $K \leqslant L$

$$\bar{u}^{(v)}_j \doteq \sum_{\mu=v}^{L-1} \breve{u}^{(\mu)}_j \frac{M^{(\mu-v)}(x_j)}{(\mu-v)!} \tag{16}$$

for $v = 0, \ldots, L-1$. $\bar{u}_j^{(v)}$ and $\breve{u}_j^{(v)}$ stand for the order v derivatives of the approximation polynomials of $\bar{u}$ and u at x_j. Note that by the Weierstrass approximation theorem it is not necessary for the approximated function $u(x)$ to be smooth. $M^{(\mu)}$ is the μth moment of the filter kernel G

$$M^{(\mu)}(x_j) = \int_{x_{j-1/2}}^{x_{j+1/2}} (x - x_j)^\mu G(x - x_j).$$

The set of Eq. (16) can be solved for $\breve{u}_j^{(v)}$ so that $\breve{u}_\mathrm{N}$ is obtained in terms of the first $L-1$ derivatives of $\bar{u}_\mathrm{N}$ and can be inserted as approximation for u_N into Eq. (7). As a result of MDEA a differential equation for the continuous extension of $\bar{u}_\mathrm{N}$ follows. The implicit SGS model can be identified by computing $\mathscr{G}_\mathrm{N}$ as defined in Eq. (7).

In this paper we focus on the one-dimensional implicit SGS model development, the extension to three-dimensional Navier–Stokes turbulence is subject of a subsequent report. As underlying conservation law we consider the viscous Burgers equation for which $F(v) = v^2/2 - v\partial v/\partial x$ is to be substituted in Eq. (1). For SGS modeling only the convective term of Eq. (3) is relevant, so that we will not consider the diffusion terms within MDEA. The exact expression for the convective part of the Burgers equation is

$$G * \frac{\partial F_\mathrm{N}(u_\mathrm{N})}{\partial x} = \bar{u}_\mathrm{N}\frac{\partial \bar{u}_\mathrm{N}}{\partial x} + \frac{1}{12}\frac{\partial \bar{u}_\mathrm{N}}{\partial x}\frac{\partial^2 \bar{u}_\mathrm{N}}{\partial x^4} - \frac{1}{720}\frac{\partial \bar{u}_\mathrm{N}}{\partial x}\frac{\partial^4 \bar{u}_\mathrm{N}}{\partial x^4}h^4 + \frac{1}{30240}\frac{\partial \bar{u}_\mathrm{N}}{\partial x}\frac{\partial^6 \bar{u}_\mathrm{N}}{\partial x^6}h^6 - + \cdots \tag{17}$$

where derivatives are to be taken at the cell centers x_N. MDEA is performed here only for equidistant meshes with $hj = h$. An analysis of the effect of varying mesh size is subject of a separate study. Results of MDEA are computed with MAPLE [1] and are given in the subsequent sections.

3.1. Implicit SGS-model adaptation for given explicit SGS model

On the example of the Smagorinsky model we demonstrate in this section how a given explicit SGS model can be matched by adjusting K and $\gamma_{k,r}^{\pm}$of the generic implicit SGS model. The Smagorinsky model formulated for the Burgers equation is

$$\tau_\mathrm{Smag} = -C_\mathrm{S}h^2\left|\frac{\partial \bar{u}}{\partial x}\right|\frac{\partial \bar{u}}{\partial x}.$$

The explicit SGS model which is inserted on the right-hand side of the filtered equations is

$$\bar{\mathscr{G}}_\mathrm{SGS} = -\frac{\partial \tau_\mathrm{Smag}}{\partial x} = 2C_\mathrm{S}h^2\left|\frac{\partial \bar{u}}{\partial x}\right|\frac{\partial^2 \bar{u}}{\partial x^2}.$$

Since the purpose here is not to assess the quality of the Smagorinsky model itself, the particular value of the Smagorinsky constant C_S is unimportant. In the following computational experiments we will use $C_\mathrm{S} = 0.2$. With the implicit SGS approach, we can identify model parameters in such a way that the resulting implicit formulation matches with the explicit model for $K = 3$ up to order $\mathscr{O}(h^3)$ as given in Table 1. Choosing $\sigma_{j+i/2} = 9C_\mathrm{S}|\tilde{u}_{j+1/2}^- - \tilde{u}_{j+1/2}^+|$ in Eq. (11), the truncation error $\mathscr{G}_\mathrm{N}$ follows as

$$\mathscr{G}_\mathrm{N} = 2C_\mathrm{S}\left|\frac{\partial \bar{u}}{\partial x}\right|\frac{\partial^2 \bar{u}}{\partial x^2}h^2 - \frac{1}{6}C_\mathrm{S}\left|\frac{\partial \bar{u}}{\partial x}\right|\frac{\partial^4 \bar{u}}{\partial x^4}h^4 + \mathscr{O}(h^6). \tag{18}$$

[1] Maple 9, Waterloo Maple Inc., 2003.

Table 1
Result for the discretization parameters $\gamma^{\pm}_{r,k}$ to match the explicit Smagorinsky model

Parameter	Value
$\gamma^{+}_{1,0}$	1
$\gamma^{+}_{2,0}$	2/3
$\gamma^{+}_{2,1}$	1/3
$\gamma^{+}_{3,0}$	3/10
$\gamma^{+}_{3,1}$	3/10
$\gamma^{+}_{3,2}$	4/10

3.1.1. Results for forced Burgers turbulence

A relevant one-dimensional model for Navier–Stokes turbulence is a properly forced Burgers equation. Here, we employ a stochastic force as suggested by Cheklov and Yakhot [32]

$$\frac{\partial v}{\partial t} + v\frac{\partial v}{\partial x} = v\frac{\partial^2 v}{\partial x^2} + f(x,t). \tag{19}$$

The solution v is 2π-periodic. As Reynolds number we choose $1/v = 10^5$. The random force $f(x,t)$ is defined in wavenumber space as

$$\hat{f}(\xi) = A\frac{\mathrm{e}^{\mathrm{i}\phi}}{\sqrt{|\xi|}\sqrt{\tau}}, \tag{20}$$

where $A = 0.04$ and $\pi \leqslant \phi \leqslant \pi$ is randomly chosen for every wavenumber and at every time step. For this forcing a dissipation scale of order $\eta \approx 10^{-3}$ follows. After an initial transient a stationary state is reached which exhibits an $\langle \hat{E}(\xi)\rangle \sim \xi^{-5/3}$ inertial range, where $\hat{E}(\xi) = |\hat{u}(\xi)|^2/2$ and $\hat{u}(\xi)$ is the Fourier transform of $\bar{u}(x)$ at wavenumber ξ. The time-step size τ is determined from Eq. (15) with CFL $= 0.5$. Time integration is performed with the TVD Runge–Kutta scheme of Shu [33].

Discretizations of Eq. (19) were integrated up to $t = 500$. Averages were gathered after a short initial transient. Fig. 2 compares the prediction of the implicit Smagorinsky model with results obtained with a spectral and dealiased discretization where the Smagorinsky model is added explicitly. We note that the prediction by the implicit Smagorinsky model agrees for the inertial-range well with that of the explicit Smagorinsky model. Discrepancies at large wavenumbers are caused by terms of order $\mathcal{O}(h^4)$ by which the implicit model differs from the explicit one.

3.1.2. Results for decaying Burgers turbulence

The solution v is L-periodic. For consistency with the results of Aldama [31] we set $v = 0.02$, $L = 500$. The initial data are computed from a distribution with initial spectrum

$$\hat{E}(\xi) = A\xi'^4 \mathrm{e}^{-a^2\xi'^2/2},$$

where $\xi' = 2\pi\xi/L$, $A = 10722.08$, $a = 19.89$. The time-step size τ is determined by Eq. (15) with CFL $= 0.5$. For reference we perform a direct simulation with a dealiased spectral discretization at a resolution of 8192 points, for which it was shown that the mesh-Reynolds number is on the order of unity [31], and a LES with a dealiased spectral discretization and an explicit Smagorinsky model.

In Fig. 3 the decay of total energy

$$E(t) = \frac{1}{2}\int_{-\infty}^{+\infty} |\hat{\bar{u}}(\xi)|^2 \,\mathrm{d}\xi \tag{21}$$

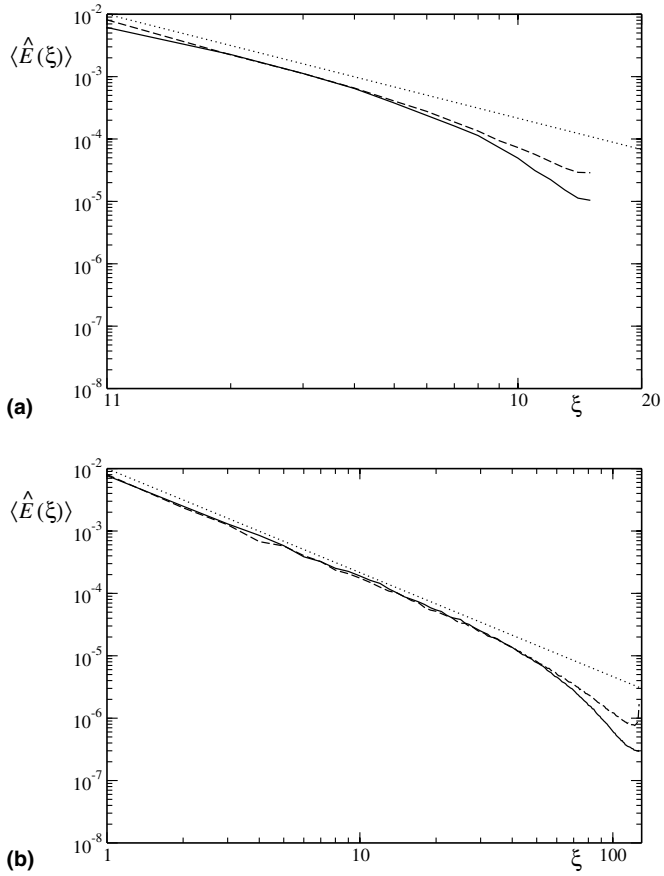

Fig. 2. Averaged energy spectra $\langle \hat{E}(\xi) \rangle$ for the stochastically forced Burgers equation: —, implicit Smagorinsky model; ----, explicit Smagorinsky model; $\cdots$, line with $\xi^{-5/3}$ rule; (a) with $N = 32$, (b) with $N = 256$.

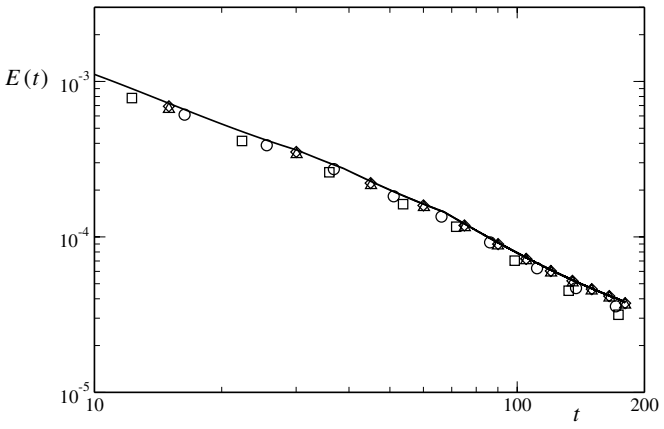

Fig. 3. Temporal evolution of total energy $E(t)$ as predicted by the implicit Smagorinsky model compared with the direct simulation —: △, implicit Smagorinsky model with $N = 256$; ◇, implicit Smagorinsky model with $N = 512$; □, explicit Smagorinsky model with $N = 256$; ○, explicit Smagorinsky model with $N = 512$.

of the different LES computations is compared with the direct simulation, showing a reasonable agreement between implicit and explicit Smagorinsky model.

For illustration we show in Fig. 4 snapshots of the solutions at time $t = 180$. Instantaneous energy spectra follow the theoretical ξ^{-2} drop-off and show again a good agreement between explicit and implicit Smagorinsky model, an example at $t = 180$ for $N = 256$ is shown in Fig. 5.

3.1.3. Effect of time integration

To check for the effect of time integration we have repeated some of the above computations with the third-order low-storage Runge–Kutta scheme of Williamson [34] and with different CFL numbers.

Fig. 6 shows for the forced Burgers case that changing the integration scheme has only very little effect on the results. Reducing the time-step size to CFL = 0.1 and to CFL = 0.01 has no visible effect on the results, Fig. 7.

A similar behavior was found for the case of decaying Burgers turbulence.

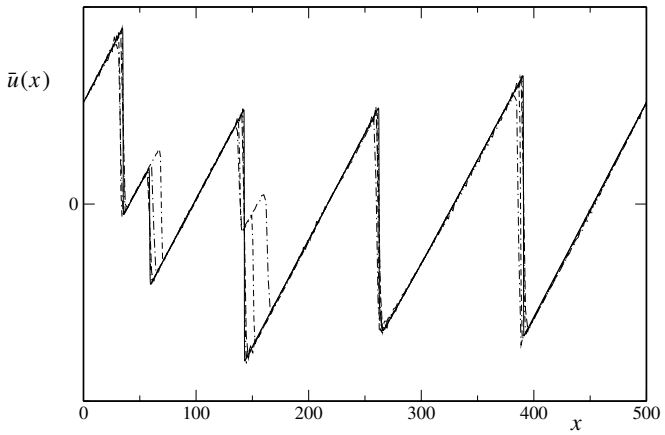

Fig. 4. Instantaneous solution compared with the direct simulation — at time $t = 180$; ----, implicit Smagorinsky model with $N = 256$; – · –, explicit Smagorinsky model with $N = 512$, — · —, implicit Smagorinsky model with $N = 256$; ·---·, explicit Smagorinsky model with $N = 512$.

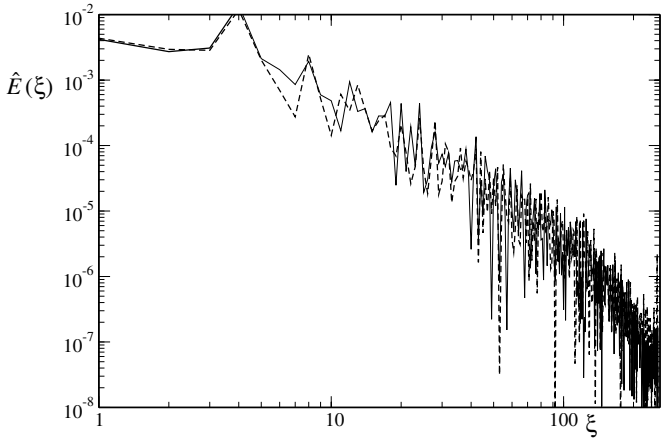

Fig. 5. Instantaneous spectra at $t = 180$ and $N = 512$: —, implicit Smagorinsky model; ----, explicit Smagorinsky model.

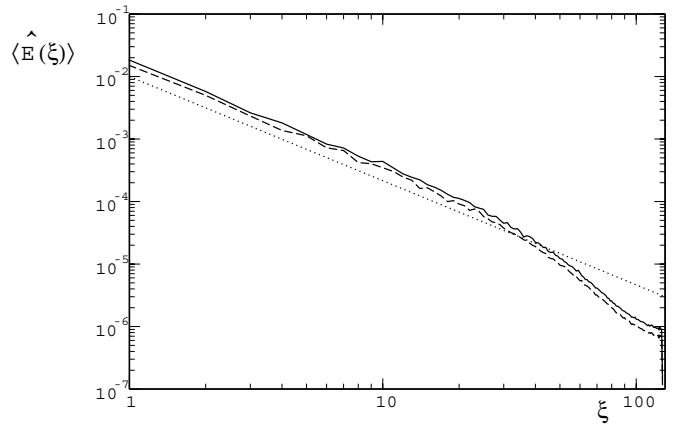

Fig. 6. Averaged energy spectra $\langle \hat{E}(\xi) \rangle$: —, implicit Smagorinsky model with TVD Runge–Kutta; ----, implicit Smagorinsky model with low storage Runge–Kutta; $\cdots$, line $\approx \xi^{-5/3}$ rule; $N = 256$.

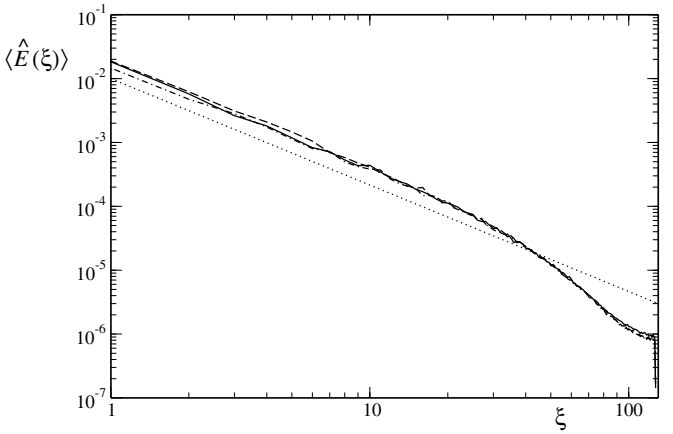

Fig. 7. Averaged energy spectra $\langle \hat{E}(\xi) \rangle$: —, implicit Smagorinsky model with CFL = 0.5; ----, implicit Smagorinsky model with CFL = 0.1; — · —, implicit Smagorinsky model with CFL = 0.01; $\cdots$, line with $\xi^{-5/3}$ rule; $N = 256$ grid points.

3.2. Implicit SGS-model construction by evolutionary optimization

Other than adjusting the model parameters $\gamma_{k,r}^{\pm}$ for a given explicit SGS model a more systematic procedure can be applied to determine these parameters. Provided that the grid resolution is sufficient, turbulent subgrid scales are believed to obey general properties such as a Kolmogorov scaling in the inertial wavenumber range for three-dimensional Navier–Stokes turbulence. Provided certain statistical properties are known one can try to find systematically the SGS model which gives the best statistical representation of the filtered scales. Optimization target is a generic reference flow configuration which represents the essential properties of flow configurations to which the SGS model will be applied. This is the basic idea of optimal LES proposed by Langford and Moser [35]. Since our model is nonlinear the stochastic estimation procedure used by Langford and Moser cannot be adapted straightforwardly to derive $\gamma_{k,r}^{\pm}$. Instead we resort to a more direct approach where an initial guess for $\gamma_{k,r}^{\pm}$ is improved by evolutionary optimization. An appropriate cost function is computed from an ensemble average of independent realizations. Since for efficiency the number of samples is

Table 2
Parameters for the evolutionary optimization algorithm

Parameter	Value
Number of genes per individual	3
Random initialization	Range from 0.0 to 0.3333
Number of generations	500
Population size	40
Offspring per generation	10
Selection of parents	Tournament, 10 members
Offspring generation	Arithmetic cross-over
New generation selection	Tournament
Mutation-variance update factor	0.95

less than what is necessary to completely remove the effect of stochastic fluctuations the resulting cost function is not smooth but exhibits residual fluctuations. Unlike standard gradient approximation-based optimization methods evolutionary algorithms can handle such non-smooth cost functions [36].

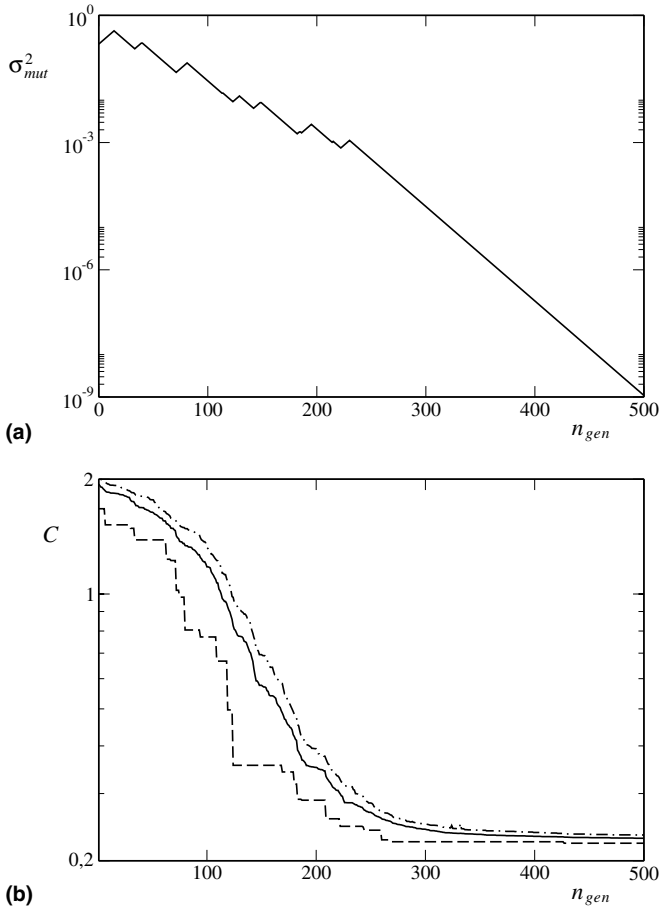

Fig. 8. Convergence histories for the stochastically forced Burgers equation monitored over 500 generations: (a) mutation variance; (b) cost function; —, average cost function; - - - -, best costfunction in ensemble; — · —, worst cost function in ensemble.

In order to simulate an evolutionary process for determining suitable parameters $\gamma_{k,r}^{\pm}$ they are considered as *genes* of an *individual* among the current *generation.* To every individual a *fitness value* determined from the cost function is assigned. In our investigation we use the following simple evolutionary algorithm, for further details the reader is referred to [36–39]:

(1) *Selection of parents*. Pairs of two datasets for $\gamma_{k,r}^{\pm}$ are drawn by a random process either with probability proportional to their fitness or by tournament selection.
(2) *Recombination*. Offspring of parents is generated by recombination of their genes. Recombination can take place either by 2-point cross-over or by arithmetic cross-over.
(3) *Mutation*. Random change of offspring genes. The random data are either normally distributed with zero mean. Their variance is adapted depending on how close the generation is to an optimum.
(4) *New generation selection*. The new generation of individuals is selected from the current generation plus offspring either by fitness selection or by tournament selection.

These four steps are looped over until an optimality criterion is satisfied or until a maximum number of generations is reached. In the following section we apply this procedure to derive an optimized parameter set for the stochastically forced Burgers equation.

For determining optimal parameters we consider the case of the stochastically forced Burgers equation as described in Section 3.1.1. Here, however, a large-scale forcing is employed which maintains a $\langle \hat{E}(\xi)\rangle \sim \xi^{-2}$ spectrum. We consider this reference case for optimization since we found that the cost-function sensitivity on the parameter set is more pronounced than for the $\langle \hat{E}(\xi)\rangle \sim \xi^{-5/3}$ case. Also, the dependency on the choice of the initial random seed is less strong which facilitates ensemble averaging. Finally, having derived optimal parameters for one case we can test their prediction quality for other cases.

We add the inverse Fourier-transform of

$$\hat{f}(\xi) = \begin{cases} A\frac{e^{i\phi}}{|\xi|\sqrt{\tau}}, & |\xi| \leqslant \xi_h/4, \\ 0, & \text{otherwise} \end{cases} \tag{22}$$

to the right-hand side of Eq. (19). In (22) $-\pi \leqslant \phi \leqslant \pi$ is randomly chosen for every wavenumber and at time t and $A = 0.04$. The cost function used for optimization is

$$C = |p - p_{\text{th}}| + \left(\frac{1}{|\xi_1 - \xi_2|} \sum_{\xi=\xi_1}^{\xi_2} (\ln\langle \hat{E}(\xi)\rangle - a - p\ln\xi)^2 \right)^{1/2}, \tag{23}$$

p and a are the parameters of the estimate $\langle \ln \hat{E}(\xi)\rangle \approx p\ln\xi + a$ which is fitted to $\langle \hat{E}(\xi)\rangle$ by a least-squares estimate over the wavenumber range $\xi_1 = 0.1\xi_h \leqslant \xi \leqslant \xi_2 = 0.9\xi_h$. The second term on the right-hand side of Eq. (23) measures the deviation from a logarithmic law, whereas the first term measures the deviation from the theoretically predicted exponent p_{th}. For the solution of the Burgers equation the periodic interval $-\pi \leqslant x \leqslant \pi$ is partitioned into $N = 128$ intervals. Time integration is performed for $0 \leqslant t \leqslant 140$ and statis-

Table 3
Result obtained by evolutionary optimization for the parameters $\gamma_{k,r}^{\pm}$, for the TV form and the WENO form of the smoothness measure $\beta_{k,r}$

Parameter	TV measure	WENO measure
$\gamma_{1,0}^{+}$	1	1
$\gamma_{2,0}^{+}$	0.000153	0
$\gamma_{2,1}^{+}$	0.999847	1
$\gamma_{3,0}^{+}$	0.000142	0
$\gamma_{3,1}^{+}$	0.001326	0
$\gamma_{3,2}^{+}$	0.998532	1

tical samples for computing the cost function are collected for $t > 7$, after an initial time transient. For all computations the time-step size is adjusted according to Eq. (15) with CFL = 0.5. Parameters of the evolutionary algorithm are summarized in Table 2.

A representative example for the convergence history of the evolutionary algorithm is shown in Fig. 8. The mutation variance decreases exponentially over the number of generations whereas the cost function decreases algebraically. For the cost function the variation over the statistical ensemble at each generation is indicated by the dashed line for the best cost function and the dash-dotted line for the worst cost function.

Optimal parameters $\gamma_{k,r}^{\pm}$ are determined for two different choices of the smoothness measure $\beta_{k,r}$, the TV form Eq. (14) and the WENO form of Jiang and Shu [30]. The resulting optimal parameters are given in Table 3. Note that for the WENO choice of the smoothness measure the stencil is effectively fixed and nonlinear effects of subgrid-scale smoothness on the candidate-stencil weights are suppressed.

Given the numerical flux function, Eq. (11), with $\sigma_{j+1/2} = |\bar{u}_{j+1} - \bar{u}_j|$ the implicit SGS model can be determined with MDEA according to Section 3 as

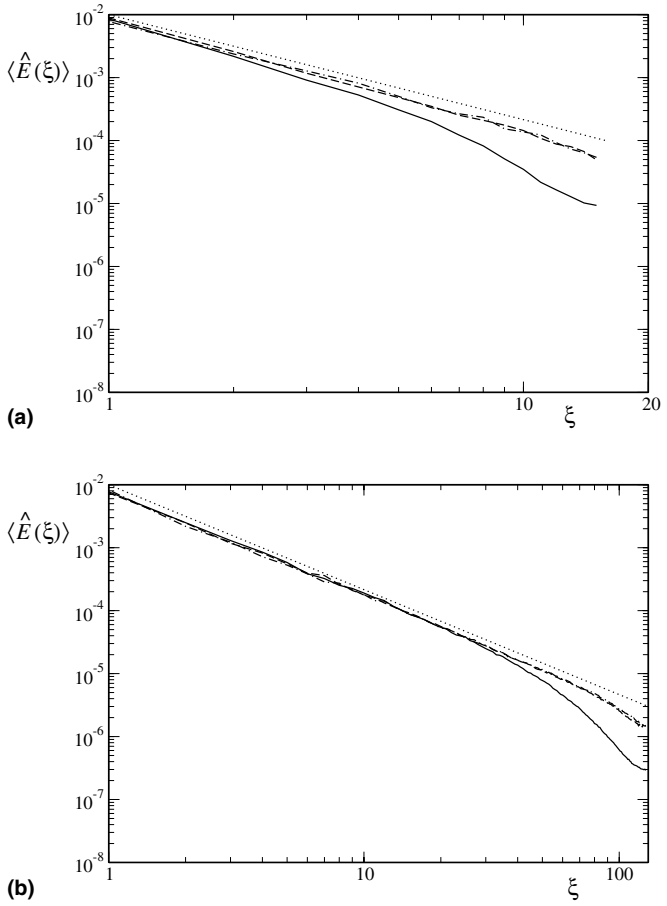

Fig. 9. Averaged energy spectra for forced Burgers turbulence with $\langle \hat{E}(\xi) \rangle \approx \xi^{-5/3}$ spectrum: (a) $N = 32$, (b) $N = 256$. —, implicit Smagorinsky model; - - - -, optimal parameters with TV smoothness measure; — · —, optimal parameters with WENO smoothness measure, · · ·, line with $\xi^{-5/3}$ rule.

$$
\begin{aligned}
\mathscr{G}_{\mathrm{N}} \doteq & \left(-0.11108 \left(\frac{\partial \bar{u}}{\partial x} \frac{\partial^2 \bar{u}}{\partial x^2} + \bar{u} \frac{\partial^3 \bar{u}}{\partial x^3} \right) + 0.66667 \left| \frac{\partial \bar{u}}{\partial x} \right| \frac{\partial^2 \bar{u}}{\partial x^2} \right) h^2 \\
& + \left(-0.00371 \frac{\partial \bar{u}}{\partial x} \frac{\partial^4 \bar{u}}{\partial x^4} + 0.16661 \frac{\left| \frac{\partial \bar{u}}{\partial x} \right|}{\frac{\partial \bar{u}}{\partial x}} \frac{\partial^2 \bar{u}}{\partial x^2} \frac{\partial^3 \bar{u}}{\partial x^3} - 0.02174 \frac{\partial^2 \bar{u}}{\partial x^2} \frac{\partial^3 \bar{u}}{\partial x^3} \right. \\
& + 0.00005 \, \bar{u} \left(\frac{\frac{\partial^2 \bar{u}}{\partial x^2}}{\frac{\partial \bar{u}}{\partial x}} \right)^2 \frac{\partial^3 \bar{u}}{\partial x^3} + 0.11095 \left| \frac{\partial \bar{u}}{\partial x} \right| \frac{\partial^4 \bar{u}}{\partial x^4} + 0.00014 \, \bar{u} \frac{\frac{\partial^2 \bar{u}}{\partial x^2}}{\frac{\partial \bar{u}}{\partial x}} \frac{\partial^4 \bar{u}}{\partial x^4} \\
& \left. + 0.00005 \frac{\left(\frac{\partial^2 \bar{u}}{\partial x^2} \right)^3}{\frac{\partial \bar{u}}{\partial x}} + 0.00010 \frac{\left| \frac{\partial \bar{u}}{\partial x} \right|}{\frac{\partial u}{\partial x}} \frac{\left(\frac{\partial^2 \bar{u}}{\partial x^2} \right)^3}{\frac{\partial \bar{u}}{\partial x}} 0.00555 \, \bar{u} \frac{\partial^5 \bar{u}}{\partial x^5} \right) h^4
\end{aligned} \tag{24}
$$

for the case of the TV smoothness measure and

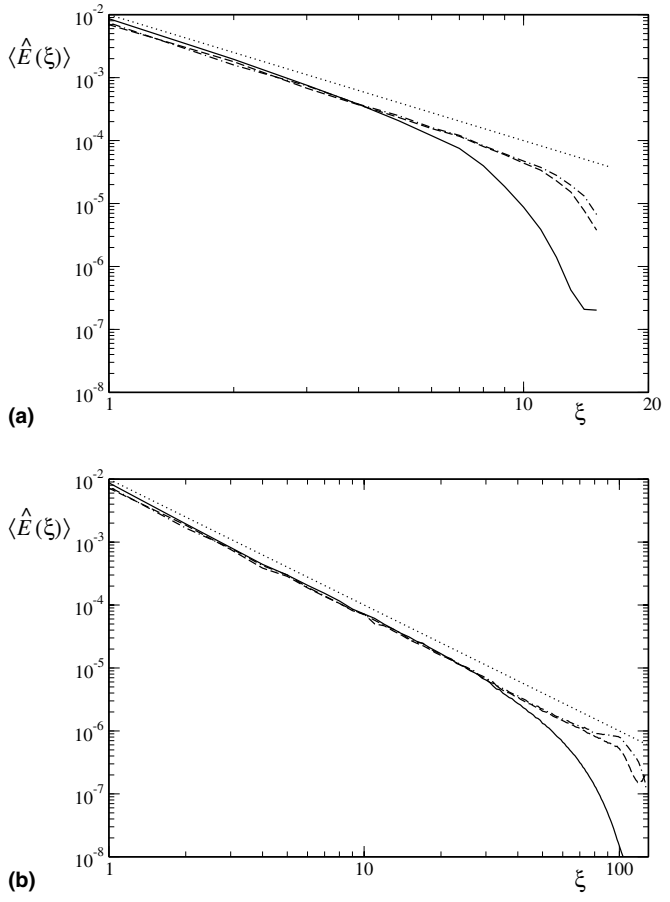

Fig. 10. Averaged energy spectra for forced Burgers turbulence with $\langle \hat{E}(\xi) \rangle \sim \xi^{-2}$ spectrum: (a) $N = 32$, (b) $N = 256$. —, implicit Smagorinsky model; ----, optimal parameters with TV smoothness measure; — · —, optimal parameters with WENO smoothness measure; ···, line $\approx \xi^{-2}$.

$$\mathcal{G}_{\mathrm{N}} \doteq \left(-0.11111 \left(\frac{\partial \bar{u}}{\partial x} \frac{\partial^2 \bar{u}}{\partial x^2} + \frac{\partial^3 \bar{u}}{\partial x^3} \bar{u} \right) + 0.66667 \left| \frac{\partial \bar{u}}{\partial x} \right| \frac{\partial^2 \bar{u}}{\partial x^2} \right) h^2 + \left(-0.00370 \frac{\partial \bar{u}}{\partial x} \frac{\partial^4 \bar{u}}{\partial x^4} + 0.16667 \frac{\left| \frac{\partial \bar{u}}{\partial x} \right|}{\frac{\partial \bar{u}}{\partial x}} \frac{\partial^2 \bar{u}}{\partial x^2} \frac{\partial^3 \bar{u}}{\partial x^3} - 0.02160 \frac{\partial^2 \bar{u}}{\partial x^2} \frac{\partial^3 \bar{u}}{\partial x^3} + 0.11111 \left| \frac{\partial \bar{u}}{\partial x} \right| \frac{\partial^4 \bar{u}}{\partial x^4} + 0.00556 \, \bar{u} \frac{\partial^5 \bar{u}}{\partial x^5} \right) h^4 \tag{25}$$

for the case of the WENO smoothness measure.

3.2.1. Results for forced Burgers turbulence

In this section, we compare the optimal implicit SGS model results with results for the implicit Smagorinsky model, as discussed in Section 3.1. Recall that the results obtained for the implicit Smagorinsky model were in reasonable agreement with those obtained with an explicit Smagorinsky model in combination with a spectral discretization.

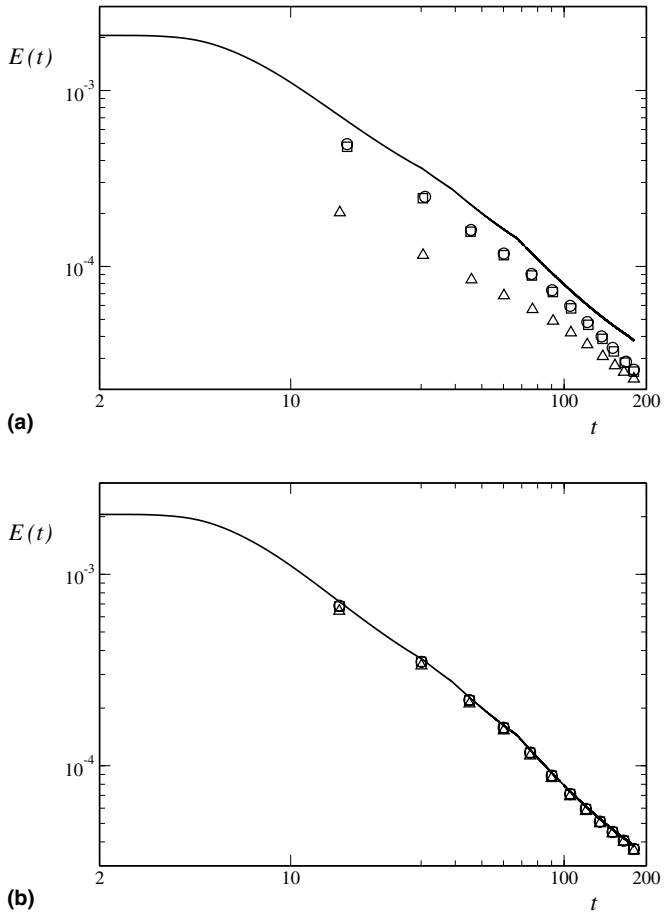

Fig. 11. Temporal decay of total turbulent kinetic energy: (a) $N = 32$, (b) $N = 256$. —, fully resolved spectral simulation; △, implicit Smagorinsky model; □, optimal parameters with TV smoothness measure; ○ optimal parameters with WENO smoothness measure.

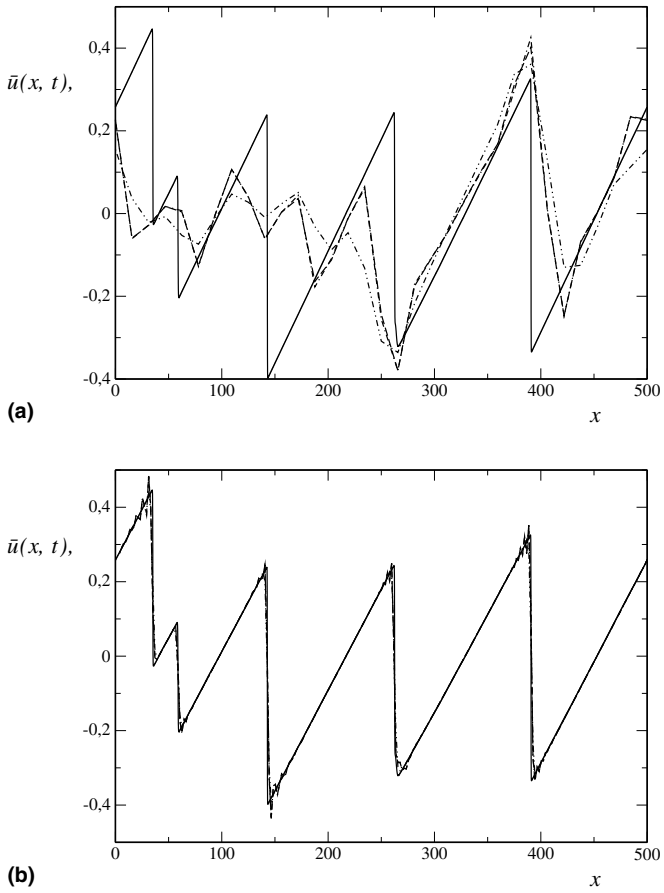

Fig. 12. Instantaneous solution for the fully resolved simulation and for the LES of decaying Burgers turbulence at time $t = 180$: (a) LES with $N = 32$, (b) LES with $N = 256$. —, fully resolved spectral simulation; — · —, implicit Smagorinsky model; - - - -, optimal parameters with TV smoothness measure; — · —, optimal parameters with WENO smoothness measure.

In Fig. 9 averaged energy spectra are shown for the case of the stochastically forced Burgers equation with $\langle \hat{E}(\xi) \rangle \sim \xi^{-5/3}$ spectrum, Eq. (20). Since the leading-order terms of the truncation error in Eqs. (24) and (25) are nearly the same the computed average spectra hardly differ for the two choices of the smoothness function. For both formulations the agreement with the theoretical spectrum is significantly better than for the implicit Smagorinsky model. Similar observations hold for the stochastically forced Burgers equation with $\langle \hat{E}(\xi) \rangle \sim \xi^{-2}$ spectrum, Eq. (22), see Fig. 10. Except for wavenumbers near ξ_h the prediction of both formulations result in very similar predictions. Near the Nyquist wavenumber the higher-order contributions of the truncation error in Eqs. (24) and (25) become more significant and cause some differences. It should be emphasized that although the optimal model parameters have been derived for the ξ^{-2}-forcing a good prediction capability is also achieved for the $\xi^{-5/3}$-forcing case.

3.2.2. Results for decaying Burgers turbulence

In this section, we apply the implicit SGS models derived above to the case of decaying Burgers turbulence, according to Section 3.1.2. In Fig. 11 the decay of total kinetic energy over time is compared between the optimal implicit SGS models with TV smoothness measure and with WENO smoothness

measure and the implicit Smagorinsky model of Section 3.1. Also for this test case the results confirm that the optimal models result in a significantly improved prediction compared with the implicit Smagorinsky model. For illustration a snap shot of the instantaneous solutions for the fully resolved simulation and the different large-eddy simulations at two different resolutions is shown in Fig. 12.

4. Conclusions

Our main objective is to demonstrate that implicit SGS models can be designed systematically and are not merely inferred by an ad hoc choice of a numerical discretization. By properly interpreting the cell-averaging and reconstruction steps of a finite-volume discretization as filtering and de-convolution, in a similar fashion as proposed recently for explicit SGS models, the instruments for designing implicit SGS models are at hand. Explicit deconvolution-type SGS models so far are limited to linear regularized de-convolution operations for the approximate reconstruction of the unfiltered field. Employing methods which are well established for ENO and WENO finite-volume discretizations we can extend the concept of approximate de-convolution to the solution-adaptive nonlinear case.

Regularization of deconvolution is achieved by limiting the degree of local interpolation polynomials. Solution adaptivity of the deconvolution is obtained by permitting all possible interpolation polynomials up to the maximum degree on admissible candidate stencils to contribute. The respective contributions are weighted by a straightforward adaptation of WENO smoothness measures. The approximately deconvolved field is inserted into a modified Lax–Friedrichs numerical flux function. These steps constitute the numerical discretization which delivers an implicit SGS model.

Similarly as the smoothness measure of WENO schemes drives the discretization to maximum order of accuracy in smooth flow regions, here the discretization is driven in flow regions of developed turbulence towards an optimized or otherwise designed truncation error. It is argued that the truncation error has the same functionality as an explicit subgrid-scale model. Up to desired order a given explicit SGS model can be matched. This is shown on the example of the Smagorinsky model. In this case the only benefit of the implicit SGS model is that no explicit computation of model terms is necessary. Implicit model parameters can, however, also be subjected to systematic optimal selection. Optimization target is a generic reference flow configuration which represents the essential properties of flow configurations to which the implicit model will be applied. Several approaches are possible, one example is the stochastic estimation. For its simplicity and robustness we have resorted, however, to evolutionary optimization. We have demonstrated that a set of optimal parameters for the case of the large-scale forced Burgers equation delivers also good results for other cases. In particular this holds for the case of a stochastically forced Burgers equation where the forcing spans the entire wavenumber range. With this forcing a resemblance of Navier–Stokes small-scale dynamics is obtained which is different from the large-scale forced or decaying Burgers solution, where the small scales are shocks. From this finding we can conclude that the observed good performance of the optimized implicit model is not merely a result of the good shock-capturing properties of the underlying WENO-like stencil weighting. It is rather a genuine SGS modeling capability of the approach which can be expected to transfer to three-dimensional Navier–Stokes turbulence. As a note in passing we remark that appropriate modifications of the smoothness measure can also be devised in order to achieve more complex responses to the local flow character. This property might be exploited for including wall modeling or transition modeling into implicit LES for the full three-dimensional Navier–Stokes equations.

The extension of the proposed implicit SGS procedure to the incompressible and compressible Navier–Stokes equations in three dimensions is subject of ongoing research and results will be reported in a subsequent paper. It is expected that also in these cases discretization parameters for the above implicit SGS model can be found which determine the behavior of the truncation error in flow regions of developed turbulence.

Acknowledgements

The presented research is supported by the German Research Council (Deutsche Forschungsgemeinschaft – DFG) in the framework of the research group FG 507. We gratefully acknowledge P. Koumoutsakos of ETH Zürich for his help on the subject of evolutionary optimization.

References

[1] J. Smagorinsky, Some historical remarks on the use of nonlinear viscosities, in: B. Galperin, S.A. Orszag (Eds.), Large Eddy Simulation of Complex Engineering and Geophysical Flows, Cambridge University Press, Cambridge, 1993, pp. 3–36.
[2] J. Smagorinsky, General circulation experiments with the primitive equations, Mon. Weather Rev. 93 (1963) 99–164.
[3] P. Sagaut, Large-eddy Simulation for Incompressible Flows, second ed., Springer, Berlin, 2002.
[4] A. Leonard, Energy cascade in large eddy simulations of turbulent fluid flows, Adv. Geophys. A 18 (1974) 237–248.
[5] J.A. Domaradzki, E.M. Saiki, A subgrid-scale model based on the estimation of unresolved scales of turbulence, Phys. Fluids 9 (1997) 2148–2164.
[6] S. Stolz, N.A. Adams, An approximate deconvolution procedure for large-eddy simulation, Phys. Fluids 11 (1999) 1699–1701.
[7] J.A. Domaradzki, N.A. Adams, Modeling subgrid scales of turbulence in large-eddy simulations, J. Turbulence 3 (2002) 24.
[8] C.D. Pruett, N.A. Adams, A priori analyses of three subgrid-scale models for one-parameter families of filters, Phys. Fluids 12 (2000) 1133–1142.
[9] S. Stolz, N.A. Adams, L. Kleiser, The approximate deconvolution model for compressible flows: decaying turbulence and shock-turbulent-boundary-layer interaction, in: R. Friedrich (Ed.), Large-eddy Simulation of Complex Transitional and Turbulent Flows, Kluwer Academic Publishers, Dordrecht, 2001.
[10] S. Ghosal, An analysis of numerical errors in large-eddy simulations of turbulence, J. Comput. Phys. 125 (1996) 187–206.
[11] A. Kravchenko, P. Moin, On the effect of numerical errors in large-eddy simulation of turbulent flows, J. Comput. Phys. 130 (1997) 310–322.
[12] T. Kawamura, K. Kuwahara, Computation of high Reynolds number flow around a circular cylinder with surface roughness, AIAA-paper 84-0340.
[13] J.P. Boris, F.F. Grinstein, E.S. Oran, R.L. Kolbe, New insights into large eddy simulation, in: Fluid Dynamics Research, vol. 10, North-Holland, Amsterdam, 1992, pp. 199–228.
[14] D.H. Porter, P.R. Woodward, A. Pouquet, Inertial range structures in decaying compressible turbulent flows, Phys. Fluids 10 (1998) 237–245.
[15] P.K. Smolarkiewicz, L.G. Margolin, MPDATA: a finite-difference solver for geophysical flows, J. Comput. Phys. 140 (1998) 459–480.
[16] J.A. Domaradzki, Z. Xiao, P.K. Smolarkiewicz, Effective eddy viscosities in implicit large eddy simulations of turbulent flows, Phys. Fluids 15 (2003) 3890–3893.
[17] C. Fureby, F.F. Grinstein, Large eddy simulation of high-Reynolds-number free and wall-bounded flows, J. Comput. Phys. 181 (2002) 68–97.
[18] E. Gamier, M. Mossi, P. Sagaut, P. Comte, M. Deville, On the use of shock-capturing schemes for large-eddy simulation, J. Comput. Phys. 153 (1999) 273–311.
[19] R.J. LeVeque, Finite Volume Methods for Hyperbolic Problems, Cambridge University Press, Cambridge, 2002.
[20] C. Fureby, G. Tabor, H.G. Weller, A.D. Gosman, A comparative study of subgrid scale models in homogeneous isotropic turbulence, Phys. Fluids 9 (1997) 1416–1429.
[21] L.G. Margolin, W.J. Rider, A rationale for implicit turbulence modeling, Int. J. Numer. Meth. Fluids 39 (2002) 821–841.
[22] N.A. Adams, The role of deconvolution and numerical discretization in subgrid-scale modeling, in: B.J. Geurts, R. Friedrich, O. Métais (Eds.), Direct and Large-eddy Simulation IV, Kluwer Academic Publishers, Dordrecht, 2001, pp. 311–320.
[23] U. Schumann, Subgrid scale model for finite-difference simulations of turbulence in plane channels and annuli, J. Comput. Phys. 18 (1975) 376–404.
[24] R. Vichnevetsky, J.B. Bowles, Fourier Analysis of Numerical Approximations of Hyperbolic Equations, SIAM, Philadelphia, PA, 1982.
[25] S. Stolz, N.A. Adams, L. Kleiser, An approximate deconvolution model for large-eddy simulation with application to incompressible wall-bounded flows, Phys. Fluids 13 (2001) 997–1015.
[26] N.A. Adams, S. Stolz, A deconvolution approach for shock-capturing, J. Comput. Phys. 178 (2002) 391–426.
[27] A. Harten, B. Engquist, S. Osher, S. Chakravarthy, Uniformly high order essentially non-oscillatory schemes, III, J. Comput. Phys. 71 (1987) 231–275.

[28] C.-W. Shu, Essentially non-oscillatory and weighted essentially non-oscillatory schemes for hyperbolic conservation laws, in: B. Cockburn, C. Johnson, C.-W. Shu, E. Tadmor, A. Quarteroni (Eds.), Advanced Numerical Approximation of Nonlinear Hyperbolic Equations, Lecture Notes in Mathematics, vol. 1697, Springer, Berlin, 1998, pp. 325–432.
[29] X.-D. Liu, S. Osher, T. Chan, Weighted essentially non-oscillatory schemes, J. Comput. Phys. 115 (1994) 200–212.
[30] G.-S. Jiang, C.-W. Shu, Efficient implementation of weighted ENO schemes, J. Comput. Phys. 126 (1996) 202–228.
[31] A.A. Aldama, Filtering Techniques for Turbulent Flow Simulation, Lecture Notes in Engineering, vol. 56, Springer, New York, 1990.
[32] A. Chekhlov, V. Yakhot, Kolmogorov turbulence in a random-force driven Burgers equation: anomalous scaling and probability density function, Phys. Rev. E 52 (1995) 5681–5684.
[33] C.-W. Shu, Total-variation-diminishing time discretizations, SIAM J. Sci. Stat. Comput. 9 (6) (1988) 1073–1084.
[34] J.H. Williamson, Low-storage Runge–Kutta schemes, J. Comput. Phys. 35 (1980) 48–56.
[35] J.A. Langford, R.D. Moser, Optimal LES formulations for isotropic turbulence, J. Fluid Mech. 398 (2001) 321–346.
[36] T. Back, D.B. Fogel, Z. Michalewicz, Handbook of Evolutionary Computation, University Oxford Press, 1997.
[37] D. Beasley, D.R. Bull, R.R. Martin, An overview of genetic algorithms: Part 1, fundamentals, University Computing 15 (1993) 58–69.
[38] D. Beasley, D.R. Bull, R.R. Martin, An overview of genetic algorithms: Part 2, research topics, University Computing 15 (1993) 170–181.
[39] S. Kern, S.D. Müller, N. Hansen, D. Büche, J. Ocenasek, P. Koumoutsakos, Learning probability distributions in continuous evolutionary algorithms – a comparative review, Natural Computing 3 (2004) 77–112.